Transmission of Leptosphaeria maculans from a cropping season to the following one

Lydia Bousset, Stéphane Jumel, Vincent Garetta, Hervé Picault, Samuel S. Soubeyrand

This file is the post-print of: Bousset (2015) Annals of Applied Botany 166: 530–543 Doi: 10.1111/aab.12205

Transmission of *Leptosphaeria maculans* from a cropping season to the following one

Bousset L[1], Jumel S[1], Garreta V[2], Picault H[1], Soubeyrand S [2]

[1] *INRA UMR1349 IGEPP, Le Rheu Cedex, France*
[2] *INRA UR546 Biostatistics and Spatial Processes, Avignon, France*

Abstract
Current modelling of inoculum transmission from a cropping season to the following one relies on the extrapolation of kernels estimated on data at short distances from punctual sources, because data collected at larger distances are scarce. We estimated the dispersal kernel of *Leptosphaeria maculans* ascospores from stubble left after harvest in the summer previous to newly sown oilseed rape fields, using phoma stem canker autumn disease severity. We built a dispersal model to analyse the data. Source strengths are described in the spatial domain covered by source fields by a log-Gaussian spatial process. Infection potentials in the following season are described in the space consisting of the target fields, by a convolution of sources and a power-exponential dispersal kernel. Data were collected on farmers' fields considered as sources in 2009 and 2011 (72 and 39 observation points) and as targets in 2010 and 2012 (172 and 200 points). We applied the Bayesian approach for model selection and parameter estimation. We obtained fat tail kernels for both data sets. This estimation is the first from data acquired over distances of 0 to 1000 m, using several non-punctual inoculum sources. It opens the prospect of refining the existing simulators, or developing disease risk maps.

Keywords: Bayesian inference; dispersal kernels; fungal spores; oilseed rape; phoma stem canker; spatial epidemiology.

Introduction
To control fungal epidemics on crops of the agro-ecosystem, the cultivation of genetically resistant varieties offers the advantage of being technically simple for the end users. However, the efficiency of varieties remains stable over time only if fungal populations do not adapt to plant host resistances (Brun *et al.*, 2010). In agro-ecosystems, crop rotations affect the presence versus absence of species within fields. These continuities and discontinuities over time and space induce cyclic epidemics (Zadoks & Schein, 1979; Bousset & Chèvre, 2012). As a consequence, adaptation of pathogen populations to host resistances has to be studied at the scale of a network of fields, during a succession of cropping seasons (Bousset & Chèvre, 2013).

To overcome the difficulty of experimentation at these scales of space and time, mathematical simulators have been developed for model-based comparison of disease management strategies (Skelsey *et al.*, 2009, 2013; Lô-Pelzer *et al.*, 2010; Hossard *et al.*, 2013). Such models are based on epidemiological knowledge. Over a succession of cropping seasons, the pathogen population dynamics consist of the succession of (a) epidemics in the field during the cropping season; (b) production of inoculum and (c) transmission of inoculum to the fields sown in the following cropping season (Bousset & Chèvre, 2012). Thus, developing models including adaptation implies describing the transmission of inoculum from a cropping season to the following one, and the dispersal of pathogen spores over field boundaries (Wingen *et al.*, 2013). This is hampered by the fact that data acquisition is difficult both by indirect and direct methods.

On the one hand, indirect approaches infer dispersal capacities from information about current population genetic structure. Some specific cases, such as in the presence of an epidemic corridor for poplar rust caused by *Melampsora laricii populina* (Xhaard *et al.*, 2012) or the presence of a change in local cline of allele frequencies for banana black sigatoka caused by *Mycosphaerella fijiensis* (Rieux *et al.*, 2013), have been used to retrieve information over a few pathogen's generations. More often, the observed differentiation pattern results from the addition of many generations (Broquet & Petit, 2009). The information derived, i.e. from the isolation by distance relationship (Rousset, 1997), cannot be directly used for modelling purposes. Further, such approaches do not always succeed for fungi (Travadon *et al.*, 2011).

On the other hand, direct approaches infer dispersal capacities from the quantification of spatial gradients. They require information at many different locations, either on propagule pressure, or on resulting disease severity. Propagule pressure can be inferred from direct spore sampling using spore traps or exposed

trap plants (Viljanen-Rollinson *et al.*, 2007). Resulting disease severity is retrieved from the quantification of symptoms. Both methods have been successfully applied at the scale of disease foci (Gregory, 1968; McHardy, 1997; Diggle *et al.*, 2002) or at field scale (McHardy, 1997; Sackett & Mundt, 2005, 2009; Soubeyrand *et al.*, 2007a; Mundt *et al.*, 2010). However, their costs and the amount of work required hamper their use over wider scales (but see Rieux, 2011).

Thus, so far, for plant pathogens only a few data sets have been collected. The modelling of dispersal among fields is either derived from aerial movement of particles (Holmes & Morawska, 2006) knowing their physical characteristics (Skelsey *et al.*, 2008, 2009; Savage *et al.*, 2011) or based on the extrapolation of empirical data collected at smaller scale, around punctual spore sources (Diggle *et al.*, 2002; Lô-Pelzer *et al.*, 2010).

In contrast, more data sets of different kind have been collected for pollen dispersal. Quantification of resulting dispersal is facilitated either when molecular markers can be used for paternity inference (Austerlitz *et al.*, 2004) or when the pollen donor source can be tracked to explain the consequences of gene flow with the use of colour markers or herbicide resistance (Damgaard & Kjellsson, 2005). The strengths and limitations can then be compared among approaches (Beckie & Hall, 2008) and these can be useful for our purpose. On the one hand, a number of reviewed empirical models simulate plot-to-plot or field-to-field pollen-mediated gene flow reasonably well (Beckie & Hall, 2008). However, towards generalisation, the main limitation stressed by these authors concerns the limited spatial and variability span of the underlying data set. First, extrapolations to a scale wider than the scale of data collection fail. Second, such inferences are dependent on the specific characteristics of the fields, as pollen transmission is dependent on plot shape and relative sizes, as well as varieties. Third, dispersal within continuous fields differs from dispersal in heterogeneous landscapes. On the other hand, a few mechanistic models have been developed for wind dispersed pollens (Beckie & Hall, 2008). They achieve predictions at short distance, for massive exchanges, but do not predict adequately the rarer events, especially at long distance.

A further limitation is the mismatch between the data collection scheme and the subsequent use of data. On the one hand, we already mentioned that when data are collected as averages over whole fields or areas, they are inherently dependent on the local landscape characteristics (Beckie & Hall, 2008). As most studies encompass only one or a few donor fields, caution is required before use over a diversity of landscapes, varieties and cropping practices. On the other hand, data on point-to-point dispersal (e.g. dispersal kernels) are more independent from the local landscape characteristics, but most of them have been collected around punctual or quasi-punctual sources (e.g. small experimental donor plots). The validity of extending them to simulate dispersal from field to field in agricultural areas, i.e. several non-punctual sources, remains to be tested. Thus, collecting data at large scale, with dispersal from several non-punctual sources, deserves further investigation. We selected phoma stem canker as a case study and developed a method to analyse such data, which could also be applicable to transmission of other diseases.

Phoma stem canker is caused by a species complex including *Leptosphaeria maculans* (Mendes-Pereira *et al.*, 2003). In France, oilseed rape is mainly grown as a winter crop, sown in late August–September and harvested in following July. In Europe, phoma stem canker is considered a monocyclic disease (West *et al.*, 2001). Epidemics are initiated in autumn, and leaf spots are observed from autumn to early spring. Stem cankers develop from spring to harvest, issued from the systemic migration of the fungal mycelium from leaf spots to leaf petiole through vessels and subsequent migration down to the stem base (Hammond & Lewis, 1986). Infected stubble ensures the carry over of the fungus from one cropping season to the next and serves as main source of inoculum. In stubble, the fungus can survive as mycelium, and two kinds of fruiting bodies can be observed on the stubble: pycnidia and pseudothecia (Ghanbarnia *et al.*, 2009, 2011). Spores produced are, respectively, conidia (pycnidiospores) passively rain splashed at short distances (Travadon *et al.*, 2007) and ascospores actively ejected, and then wind dispersed (Marcroft *et al.*, 2004).

The aim of our study was to collect data on *L. maculans* spore dispersal in a commercial situation and to develop methods for their analysis. In autumn, ascospores of the fungus produced on stubble left after harvest the previous summer (sources) are disseminated to newly sown oilseed rape fields (targets). During autumns 2009–2012, we assessed phoma stem canker disease severity in farmers' oilseed rape fields, with several inoculum sources and several targets. To estimate the dispersal kernel of ascospores, we built a dispersal model by following the approach of Soubeyrand *et al.* (2007b) for constructing epidemic models,

and fitted the model to available phoma data. The model is a mechanistic-statistical model (Berliner, 2003; Wikle, 2003; Soubeyrand *et al.*, 2009a, 2009b) that combines (a) a probabilistic description of the source intensities spread in source fields, (b) a quasi-mechanistic description of the dispersal and (c) probabilistic descriptions of the observations in source fields and target fields. Thus, we built a spatial state-space model depending on an unknown latent Gaussian spatial process (Diggle *et al.*, 1998) and unknown parameters with biological meanings. These unknown components were estimated using the Bayesian approach via a Markov chain Monte Carlo (MCMC) algorithm (Diggle *et al.*, 1998; Marin & Robert, 2007; Bourgeois *et al.*, 2012).

Materials and methods

Oilseed rape cultivation in the area

Farmers' oilseed rape fields were located near Le Rheu (Ille et Vilaine, France; 48 1°N, 1 5°W) a region with rather small fields, often with hedges comprising high trees. From each farmer, we obtained authorisation to perform disease assessment, but we neither selected fields for specific cultivation (rotation, cropping practices, varietal choice and disease management) nor required any changes from the farmer's cultivation choices. In the area, winter oilseed rape is generally sown in late August–September and harvested in July. Depending on the year and the field, mild to severe phoma stem canker epidemics develop in the autumn, resulting in variable numbers of cankered plants at harvest (Brun *et al.*, 2010). The climate in the area is oceanic, and meteorological data were obtained from the INRA CLIMATIK database, for Le Rheu weather station.

Fields assessed

Fields were assessed in autumn for phoma leaf spots severity (see below), with a total of 1421 observations. We characterised two transmission events, hereafter called ‘transmission 2010’ and ‘transmission 2012’. For each, we assessed severity both on source fields (2009 and 2011) and on target fields (2010 and 2012), respectively (Table 1). A subset of the existing fields was observed, and observation points in observed fields were approximately regularly scattered to cover the whole fields (the sampling was higher near borders of some target fields in contact with source fields). At each observation point, depending on the year, one or two observers performed one or two assessments.

Coordinates at each observation point were saved with a portable Global Positioning System. Coordinates at nodes along field edges were marked on IGN aerial pictures (BD Ortho®IGN, Paris, France) and retrieved with Quantum GIS (1.8.0).

Table 1. *Numbers of existing and observed fields considered either sources or targets in our analysis, observations points and disease intensity, for each cropping season*

		Number of Fields		Observation Points[b]			Disease Severity[c] (Mac.m2)			
Cropping Season[a]	Status	Existing	Observed	Number	Data per Point	Dates of Observation	Mean	SD	Min	Max
2009–2010	Sources	11	5	72	1–2 obs × 1 assess	26 November to 14 December 2009	31.0	21.7	3	96
2010–2011	Targets	10	10	172	2 obs × 2 assess	29 November to 17 December 2010	17.6	21.4	0	136
2011–2012	Sources	12	3	39	2 obs × 2 assess	7 November 2011	0.8	1.9	0	15
2012–2013	Targets	16	11	200	1 obs × 2 assess	26 October to 30 October 2012	15.3	23.5	0	165

[a] The cropping season is from sowing (late summer) to harvest (early summer).
[b] At each observation point, one or two observers performed one or two observations, depending on the cropping season. ‘obs’ stands for ‘number of observers’ and ‘assess’ stands for ‘number of assessments per observer’.
[c] Disease severity is assessed as the number of leaf spots counted in a 1 m^2 area observed during 1 min. Mean, standard deviation, minimum and maximum are indicated for each season.

Observation processes

Disease severity was quantified using the ‘Mac.m2’ estimator, i.e. counting the number of phoma leaf spots seen within 1 min on 1 m^2. This estimator yields a continuous numerical variable, correlated to the number of leaf spots per plant, but being much faster to implement than such a count per plant (Bousset *et al.*, personal communication). Mac.m2 were scored on days with constant luminosity. For each observation point, a 0.5 m × 2 m observation zone was delimited with a polyvinyl chloride pipes structure, placed at canopy height. Yellow leaves were few, and leaf lesions were not counted on them.

For the counting, the observer moved at regular speed sidewise along the length of the observation zone. A timer was used to standardise the observation time to 1 min. Within one field, the observer moved always along the same border of the observation zone to keep light orientation constant. The observer was careful in maintaining regular speed whatever the number of leaf lesions was, without accelerating when scarce, or slowing down when plenty.

Mechanistic model

Here, we introduce the two following model components: the strengths of pathogen sources in source fields and the infection potential that pathogen sources generate in target fields.

The source strengths in source fields are modelled by a log-Gaussian stationary spatial process Λ_S with an exponential power auto-covariance function (Yaglom, 1987, pp. 364–365); the subscript S means source. Thus, for a set of n sites $y_1, \ldots, y_n$ located in source fields, $\log\{\Lambda_S(y_1), \ldots, \Lambda_S(y_n)\} \sim \text{Normal}\{(\mu, \ldots, \mu), \Sigma\}$ where $\mu \in \mathbb{R}$ is the mean parameter of the log-source strengths, Σ is their variance-covariance matrix whose element (j, j') is equal to $\sigma_1^2 \exp\left(-\sigma_2 \left\| y_j - y_{j'} \right\|^{\sigma_3}\right)$, wherein σ_1^2, σ_2 and σ_3 are the variance parameter, the range parameter and the smoothness parameter of the covariance function, respectively, and $\|.\|$ is the Euclidean distance in the space $\mathbb{R}^2$.

The infection potential, that gives a measure of the risk of infection in target fields, is modelled by a convolution Λ_T between the source strengths Λ_S and an exponential power dispersal kernel K (Austerlitz *et al.*, 2004); the subscript T means target. Thus, for any site x located in a target field, $\Lambda_T(x) = \int_{\mathbb{R}^2} \Lambda_S(y) K(x-y)\,\mathrm{d}y$

$K(x-y) = \dfrac{\beta_2}{\beta_1^2 \Gamma(2/\beta_2)} \exp\left\{-\left(\|x-y\|/\beta_1\right)^{\beta_2}\right\}$, where $\Lambda_S(y)K(x-y)$ represents the contribution of the pathogen source located at site y to the potential infection at site x, and where β_1 and β_2 are the scale and shape parameters of the dispersal kernel.

Models of the observation processes

Disease severities in source fields noted $Y_{S,i}$, $i = 1, \ldots, n_S$, (i.e. counts of phoma leaf spots seen within 1 min on 1 m^2) are assumed to be drawn under independent Poisson distributions with means proportional to the source strengths at sites $x_{S,1}, \ldots, x_{S,n_S}$ where the severities were measured: $Y_{S,i} \underset{\text{indep.}}{\sim} \text{Poisson}\{\alpha_1 \Lambda_S(x_{S,i})\}$ where $\alpha_1 > 0$ is a proportionality parameter.

Disease severities in target fields noted $Y_{T,i}$, $i = 1, \ldots, n_T$, (i.e. counts of phoma leaf spots seen within 1 min on 1 m^2) are assumed to be drawn under independent negative binomial distributions with means proportional to the infection potentials at sites $x_{T,1}, \ldots, x_{T,n_T}$ where the severities were measured: $Y_{T,i} \underset{\text{indep.}}{\sim} \text{negative binomial}\{\alpha_2 \Lambda_T(x_{T,i}), \theta\}$ where $\alpha_2 > 0$ is a proportionality parameter and $\theta > 0$ is an overdispersion parameter. Here, the negative binomial distribution is used to counterbalance the regularisation due to the convolution defining Λ_T. Indeed, for disease severities in source fields, the combination of the log-Gaussian randomness in Λ_S and the Poisson randomness leads to a given level of stochasticity. In contrast, Λ_T, that is defined as a convolution between Λ_S and K, has a lower level of variability than Λ_S. To counterbalance this, we used a negative binomial distribution whose realisations are more variable than those of a Poisson distribution with the same mean. This probabilistic trick is a parsimonious manner to obtain the same level of stochasticity in source and target fields. Alternative approaches related to biological processes are presented in the Discussion section.

Bayesian inference – estimation

The combination of the mechanistic model and the models of the observation processes defined above leads to a mechanistic-statistical model or a state-space model (Berliner, 2003; Wikle, 2003; Soubeyrand *et al.*, 2009a, 2009b) whose structure is summarised in Fig. 1. The model parameters and latent variables were estimated via a Markov chain Monte Carlo algorithm with Metropolis-Hastings sampler (Marin & Robert, 2007). The vector of unknown parameters is $(\mu, \sigma_1, \sigma_2, \sigma_3, \beta_1, \beta_2, \alpha_1, \alpha_2, \theta)$. The latent variables correspond to

values of Λ_S. For the sake of tractability, we discretised the space formed by source fields: the discrete space is formed by the intersection of the polygons delimiting the source fields and a regular square grid covering the study area, and we only used the values of Λ_S at the n_G nodes $x_{G,1}, \ldots, x_{G,n_G}$ of the resulting grid; the subscript G means grid. Thus, the convolution $\Lambda_T(x) = \int_{\mathbb{R}^2} \Lambda_S(y) K(x-y)\,dy$ was replaced by the finite sum $\Lambda_T(x) = \sum_{j=1}^{n_G} \Lambda_S(x_{G,j}) K(x - x_{G,j})$, the stochastic model for disease severities in source fields $Y_{S,i} \underset{\text{indep.}}{\sim} \text{Poisson}\{\alpha_1 \Lambda_S(x_{S,i})\}$ was replaced by $Y_{S,i} \underset{\text{indep.}}{\sim} \text{Poisson}\{\alpha_1 \Lambda_S(x_{G,nn(i)})\}$ where $x_{G,nn(i)}$ denotes the nearest neighbour (based on the Euclidean distance) of $x_{S,i}$ among sites $x_{G,1}, \ldots, x_{G,n_G}$, and the latent variables to be estimated are $\{\Lambda_S(x_{G,1}), \ldots, \Lambda_S(x_{G,n_G})\}$.

Figure 1 *Direct acyclic diagram of the dispersal model. Observations Y_S in source fields depend on the source strengths Λ_S and the proportionality parameter α_1. Λ_S is a log-Gaussian spatial process with mean μ and covariance matrix parameterized by (σ_1, σ_2, σ_3). Observations Y_T in target fields depend on the infection potential Λ_T, the proportionality parameter α_2 and the overdispersion parameter θ. Λ_T is the convolution between the source strengths Λ_S and a dispersal kernel parameterized by (β_1, β_2). Parameters τ are the parameters of the prior distributions of the model parameters (see Table S1).*

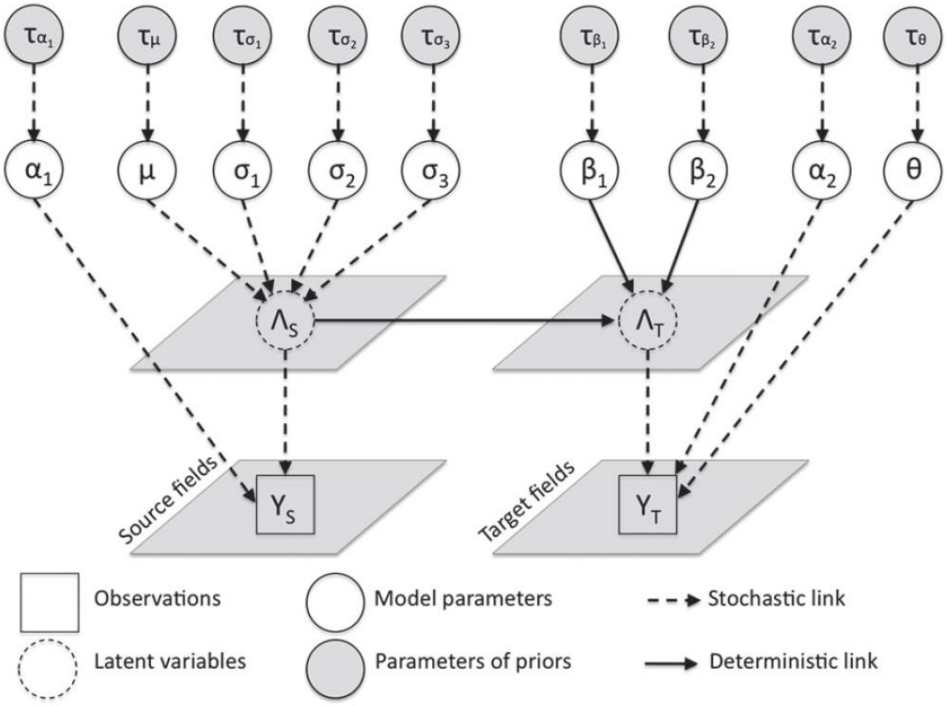

The MCMC algorithm that was developed was similar to those developed by Diggle *et al.* (1998) and Bourgeois *et al.* (2012) for a hierarchical spatial model with a latent Gaussian vector. Table S1, Supporting Information, provides complete information about prior and proposal distributions. Here, we only mention the most significant points. We arbitrarily fixed $\alpha_1 = 1$ because α_1 and α_2 are not both identifiable because of the form of the model (strong prior information on either α_1 or α_2 should be used to obtain biologically meaningful estimates of these parameters). We used different fixed values for the smoothness parameter σ_3 of the exponential power auto-covariance function and for the shape parameter β_2 of the dispersal kernel because of MCMC convergence issues (values for σ_3: 0.5, 1.0 and 1.5; values for β_2: 0.02, 0.05, 0.08, 0.10, 0.15, 0.20, 0.50, 1.00 and 2.00). The values that were used for β_2 cover a range sufficiently large to fit the model to data with both thin- and fat-tailed dispersal kernels. We used vague prior distributions for the other parameters (μ, σ_1, σ_2, β_1, α_2, θ). For each value tried for (σ_3, β_2), we performed 10 MCMC runs. For each run, one million iterations were performed, the first 50 000 iterations were discarded for the burn-in, and the chain was sub-sampled every 500 iterations to get a posterior sample.

To draw maps of the infection potential Λ_T, we need to complete the MCMC runs with a post-processing analysis. To interpolate Λ_T over a grid covering target fields, we provide for each node x of this grid the posterior sample of $\Lambda_T(x)$ by computing $\Lambda_T(x) = \sum_{j=1}^{n_G} \Lambda_S(x_{G,j})\, K(x - x_{G,j})$ at each saved iteration of the MCMC run.

Bayesian inference – model selection

By trying different fixed values for σ_3 and β_2, we fitted different models; i.e. one model for each value of (σ_3, β_2). Therefore, we carried out a model selection procedure using the Bayes factor computed with the harmonic mean estimator (Kass & Raftery, 1995). To get robust assessment of the Bayes factor, we used, for each value of (σ_3, β_2), the mean of the 10 harmonic mean estimates obtained for 10 MCMC runs).

Results

Disease severity data

Brittany has an oceanic climate (Fig. S1) with mild temperatures, in the range 3–20°C for monthly average, and rainfall throughout the year, in the range 550–900 mm per year from 2009 to 2012 (Fig. S1). In autumn, which is the period of *L. maculans* spore dispersal, both mean hourly wind distance and temperature peak in early afternoon (Fig. S2). In autumn, wind prevalent direction and cumulative wind distance vary depending on the year and month (Fig. S3).

From 2009 to 2012, meteorological contexts (Figs S1–S3), crop development and inoculum availability resulted in epidemics of contrasting severities (Table 1). Within each year, variation among fields and among observation points was high (Fig. 2). Disease severities in target fields generally increased with decreasing distance to source fields.

Figure 2 *Spatial representation of observed measurements of disease intensities (Mac.m2) in source plots and target plots for the transition 2010 (upper panel, cropping season 2009–2010 to 2010–2011) and the transition 2012 (lower panel, cropping season 2011–2012 to 2012–2013) data sets, after spatial anonymisation. Circles represent sampling points, colored according to disease severity. Disease has not been quantified in the fields containing no circles.*

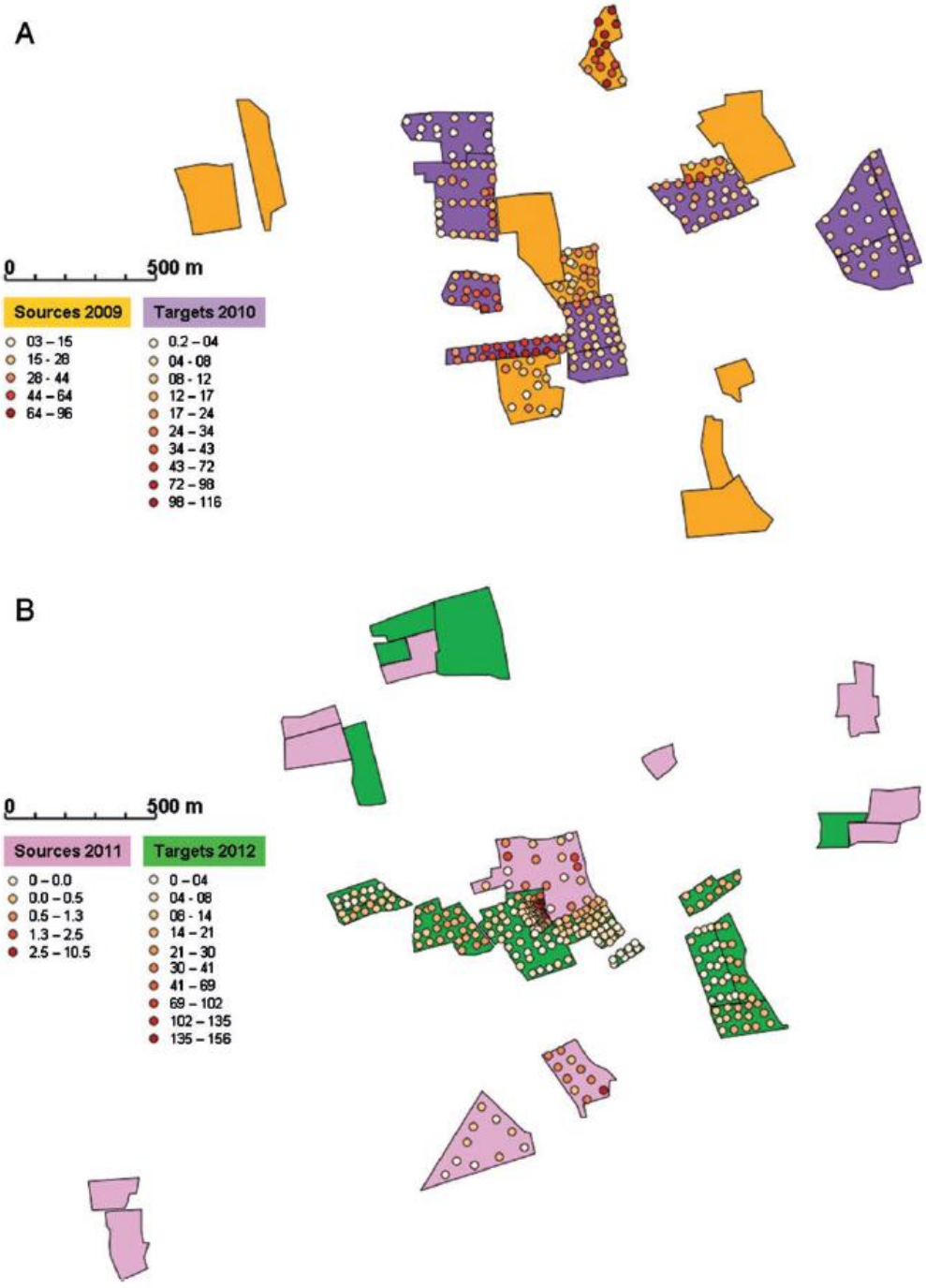

Model selection

The different versions of the model were fitted independently to the transition 2010 and to the transition 2012 data sets. In both cases, the smoothness parameter σ_3 of the covariance function had only a marginal influence, whereas the shape parameter β_2 of the dispersal kernel had a major influence (Fig. 3). The models with the highest value of Bayes factor were in both cases with fat-tailed kernels. For the 2009–2010 data, we selected the model with $\beta_2 = 0.08$ and $\sigma_3 = 0.5$. For the 2011–2012 data, we selected the model with $\beta_2 = 0.15$ and $\sigma_3 = 0.5$. For these selected models, Figs S4 and S5 give the posterior distributions of model parameters. It has to be noted that the differences in the Bayes factors for β_2 between 0.05 and 0.15 are low for both data sets.

Therefore, based on our analysis, we cannot state that β_2 is significantly different in 2010 and 2012 (note that convergence issues of the MCMC when β_2 was estimated did not allowed us to rigorously test this difference).

Figure 3 *Logarithmic values of Bayes factors[a] for the selection of the best model for the 2009–2010 (left) and the 2011–2012 data sets. For each of the three shape parameter of the covariance function (0.5; 0.1; 1.5, respectively), 12 and 9 values of the shape parameter of the dispersal kernel were tested, respectively. For each model tested, the difference with the Bayes factor of the best model (set to zero) is indicated. [a]The Bayes factor is used to compare two models. Higher the Bayes factor, better the model. The harmonic mean of the likelihood values was used to assess the Bayes factors (Kass & Raftery, 1995, Section 4.3).*

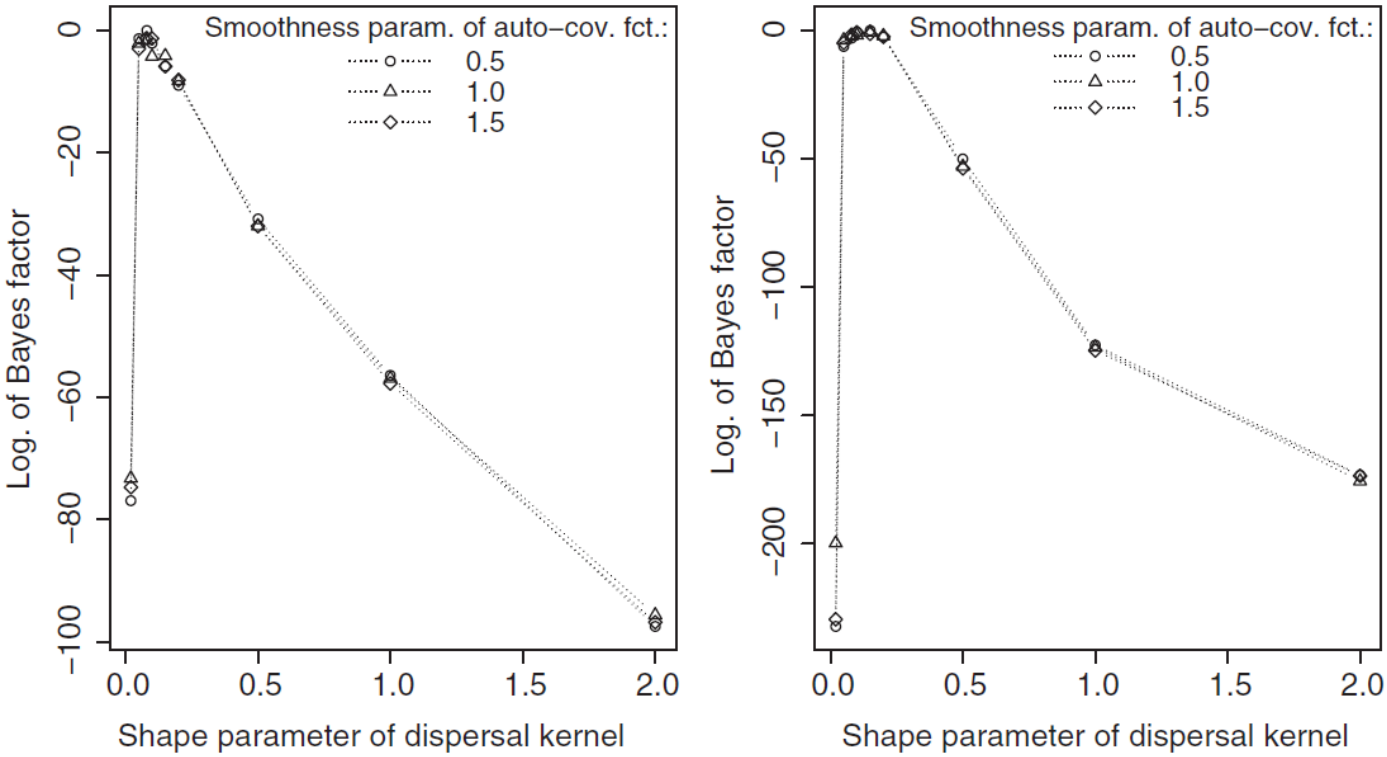

Spatial reconstruction of source strength and infection potential, and validation

Using the selected models, we drew maps of source strength and infection potential for both data sets (Figs 4 and 5, left panels). These maps also show estimations of source strength and infection potential in unobserved source fields and target fields, respectively. It has, however, to be noted that the uncertainty in these fields is large (Figs 4 and 5, right panels). For both data sets, reconstructed maps show variation in disease intensities among and within fields, as was observed in the data (Fig. 2). Strengths of infection sources vary among source fields. Highest predicted infection potentials occur close to source fields (Figs 4 and 5).

Figure 4 *Spatial representation of posterior medians (left) and posterior standard deviations (right) of disease intensities in source plots (top) and target plots (bottom) for the transition 2010 (cropping season 2009–2010 to 2010–2011) data set, after spatial anonymisation. Sources are marked out in red and targets in black.*

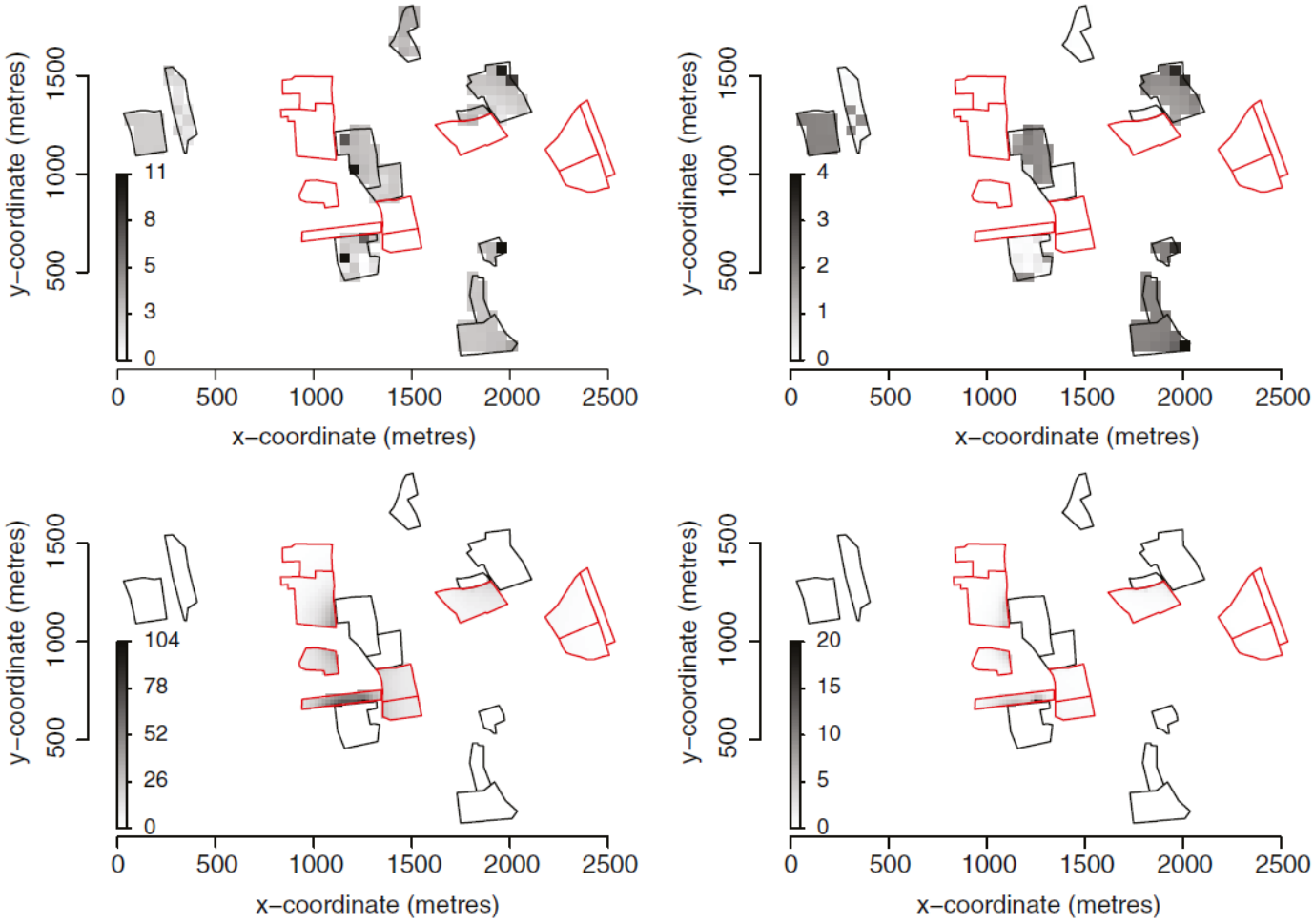

We validated the model in its ability to reconstruct source strength and potential infection by comparing the observed values of severities in source and target fields with the posterior distributions of their predictions (details are given in legends of Table S2 and Figs S6 and S7). Concerning pathogen sources, the combination of the log-Gaussian spatial process and the Poisson distribution adequately represents the variation of disease severities. Concerning observations in target fields, the combination of the convolution (between the log-Gaussian spatial process and the dispersal kernel) and the negative binomial distribution adequately represents the variation of disease severities, but underestimates in expectation large disease severities in 2010 (Fig. S8). The sites where underestimation occurs are spatially aggregated but are at various distances from source plots. This point and the fact that we used a very flexible class of dispersal kernels tend to indicate that the underestimation in expectation of large disease severities in 2010 is not due to the dispersal kernel. Possible explanations for the underestimation are proposed in the Discussion section.

Figure 5 Spatial representation of posterior medians (left) and posterior standard deviations (right) of disease intensities in source plots (top) and target plots (bottom) for the transition 2012 (cropping season 2011–2012 to 2012–2013) data set, after spatial anonymisation. Sources are marked out in red and targets in black.

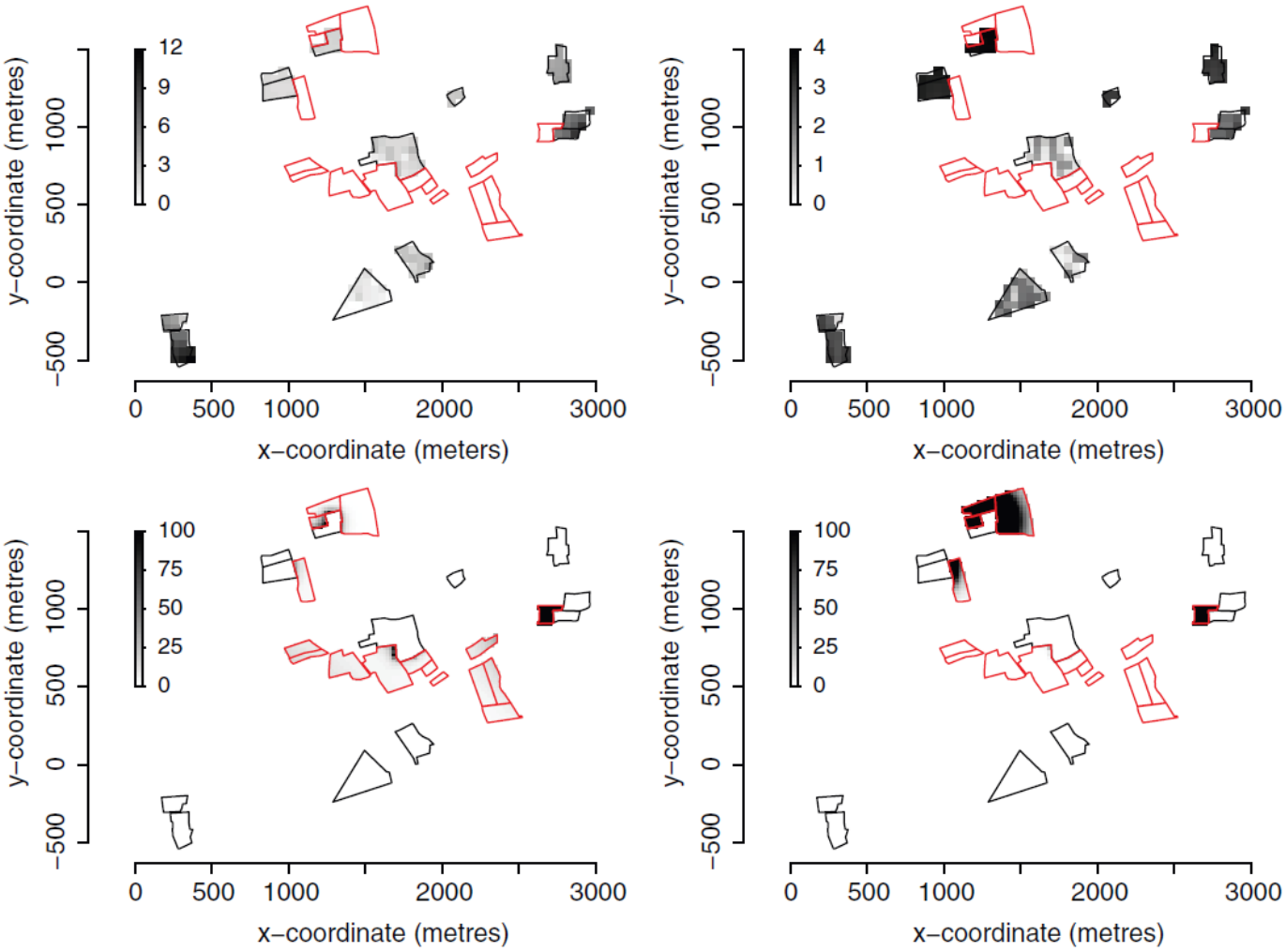

Estimation of dispersal kernel

Posterior median values of the two dimensional dispersal kernel at increasing distances were obtained (Fig. 6). Both kernels have similar values at distances up to 100 m. At larger distances, values issued from the 2010 kernel are higher than values from the 2012 kernel. Examples of kernels used in Lô-Pelzer *et al.* (2010) were represented for different wind speeds, selected in the range of observed hourly wind velocities at le Rheu in autumn 2010 and 2012 (Fig. 6). The latter kernels tend to underestimate dispersal at short distances for increasing wind speeds. On the contrary, for wind speed from 1 to 20 m s^{-1}, kernels fall between the two estimated in our study.

Discussion

For two transitions from one cropping season to the next, we have collected two data sets around several non-punctual sources, with detailed observations at distances from 0 to 1000 m. For phoma stem canker, decrease of disease severity had only been evaluated along single linear transects with increasing distance from two source fields (Marcroft *et al.*, 2004) and one adjacent source fields (Hammond & Lewis, 1986). Our study confirms that most ascospores fall within distances of 10th of metres. However, when numbers produced are large, some will travel further.

At landscape scale, one data set of disease severity data averaged over 1 ha areas had been collected in commercial fields of two successive cropping seasons in Australia (Marcroft *et al.*, 2004). However, averaging over fields does not alleviate the dependence on the spatial configuration of sources and targets in the landscape, for example their relative sizes and relative positions (Beckie & Hall, 2008). Retrieving information

on point-to-point dispersal from several sources at landscape scale offers the advantage of averaging over several conditions (varieties, cropping practices), and removing some of the influence of the spatial configuration of sources and targets.

Figure 6 *Posterior median of the value of the two dimensional dispersal kernel at increasing distances for the 2009–2010 dataset (solid black line) and the 2011–2012 dataset (dashed black line). Dotted lines are the corresponding posterior quantiles of levels 0.025, 0.1, 0.25, 0.75, 0.9 and 0.975, from bottom to top lines. Red lines are examples of kernels used in the simulator of Lô-Pelzer et al. (2010) with speed equal to 0.1, 1, 5 and 20 m* s^{-1} *(indicated beside red lines).*

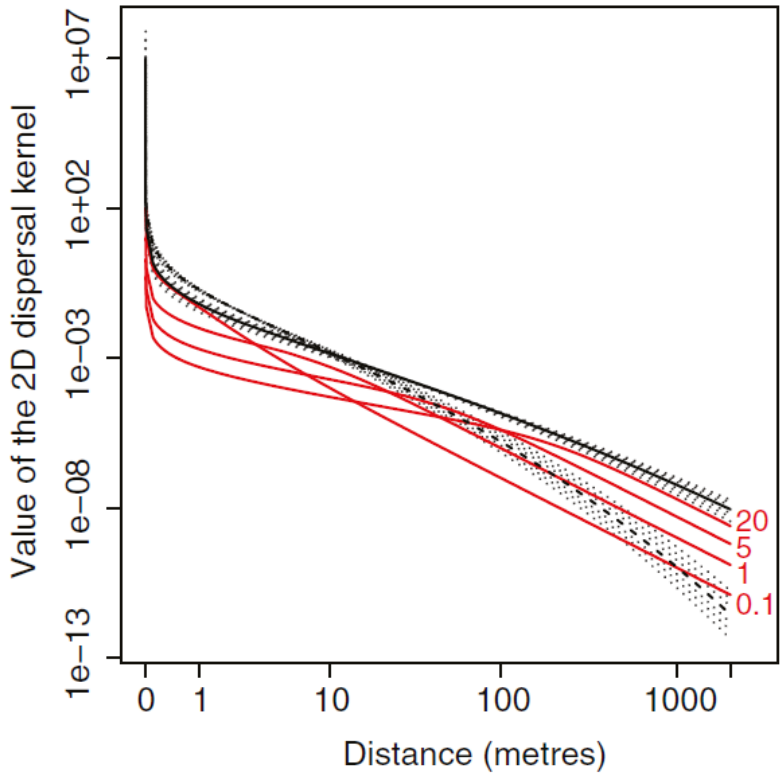

Available studies using mechanistic models contradict the idea that information on dispersal can be fully independent from the studied area. First, the climatic regime shows broad differences between regions. From simulations under West-Australian Mediterranean climate, meteorological variables such as sensible heat flux, mean horizontal wind speed, friction velocity and temperature, show a diurnal pattern with large variations, which may affect the proportion of spores that undergo long distance dispersal (Savage *et al.*, 2012). Our study has been performed in Brittany, with an oceanic climate (Figs S1–S3). Repeating such observations in contrasting regions is thus desirable before use of the estimated dispersal parameters in different climatic regions. Second, the biological characteristics of the fungi interacting with dissemination capacity may be region specific. From their simulation work, Savage *et al.*, (2013) conclude that the time of spore emission interacts with weather variables to determine achieved dispersal. They report that for *L. maculans*, available studies indicate that diurnal pattern of spore discharge differs between England, Canada and Australia. Because reaching target fields is required for survival of the fungus over years, they even postulate that discharge pattern may be under selection. This may especially be the case in areas where average distance between stubble and newly emerging oilseed rape seedlings is large. Thus, dispersal of ascospores up to 8 km (Bokor, 1975) may be quite higher than in areas with frequent adjacent source-target fields as in our study.

Nevertheless, both in transition 2010 and 2012, the best fit was achieved for a ‘fat tail’ dispersal kernel. This is coherent with existing datasets for fungi (Mundt *et al.*, 2009). For *L. maculans*, the exponential power kernel we provide offers the advantage over the previously used half-Cauchy (Diggle *et al.*, 2002; Lô-Pelzer *et al.*, 2010) of being defined at the origin, allowing for a better precision at short distances. The design of our

study does not accommodate long distance dispersal (Wingen *et al.*, 2013), and this would add to the benefit of the fat tail kernel. Theoretical predictions and empirical data (Mundt *et al.*, 2009) indicate that fat tail kernels yield accelerating waves at the epidemic front. *L. maculans* was indeed able to expand its repartition area both in Canada (Dilmaghani *et al.*, 2009) and in Eastern Europe (West *et al.*, 2001), two regions where only *Leptosphaeria biglobosa* was previously reported. The speed of epidemic front progress has been estimated at 17 km per year across Canada (Zhang *et al.*, 2014), under the assumption of a constant wave speed. Considering spatial extension of disease, a noticeable difference remains between pollen grains and fungal spores. Upon dispersal of few particles at long distance, the pollen grains most of the time reach plants emitting pollen themselves, thus pollen competition occurs. However, the fungal spores may reach uninfected plants, without competition among spores during infection. Thus, the fungal epidemic front progress may proceed for even low numbers of dispersed particles.

In our analysis, the comparison of model predictions with observed data (Table S2 and Figs S6–S8) indicated that the data fit was correct, although several directions could be explored to improve it, especially reconsidering three of our hypotheses as follows.

The first hypothesis is uniform receptivity of target fields. When varieties with efficient resistance gene combinations are deployed, receptivity of the crop to *L. maculans* is largely impacted (Brun *et al.*, 2010). In recent years, oilseed rape varieties with the efficient RLm7 genes are deployed (Pinochet, 2009; Leflon, 2013). On such varieties, fewer leaf spots appear than on susceptible varieties, for similar numbers of deposited spores. Contrasted cropping practices with respect to sowing time and fertilisation may further alter receptivity (Aubertot *et al.*, 2004). Thus, target fields at similar distances from a given source may have different disease severities, altering the data fit. Combining disease severity data with information on varieties and cropping practices remains to be explored.

The second hypothesis is proportionality in expectation between (a) disease severity observed in source fields and (b) quantity of inoculum locally emitted (i.e. where disease severity was observed). Buried stubble does not emit spores, and stubble decomposition is altered depending on summer cropping practices (Turkington *et al.*, 2000). Further, we characterised source strength at the leaf spot stage. Genetic quantitative resistance of the varieties interferes with the systemic migration of the fungus from leaf spots downwards to stem base, yielding different necrosis severities (Delourme *et al.*, 2006). Fructification intensity increases with increasing necrosis severity (Lô-Pelzer *et al.*, 2009). Combining autumn severity data with information on subsequent migration of the fungus towards stem basis remains to be explored.

The third hypothesis is isotropy and independence of spore dispersal. We considered the dispersal of individual spores as independent, although wind gusts promote the joint dispersal of particles that result in anisotropic dispersal because neither wind direction nor intensities are stable over time. Anisotropic dispersal has been documented for plant fungi at the field scale and beyond (Sackett & Mundt, 2005; Soubeyrand *et al.*, 2007a, 2009c; Rieux *et al.*, 2014). Simulation studies indicate that anisotropic kernels allow a better prediction of the tail, compared to isotropic kernels (Savage *et al.*, 2011). Dispersal models allowing anisotropy may thus improve the quality of prediction. In our analysis, the negative binomial noise accounts for anisotropy. But if it were feasible to achieve sufficient observation coverage for the purpose, one could model anisotropy explicitly. In addition, group dispersal models have been developed to take into account the joint dispersal of spores with wind gust (Soubeyrand *et al.*, 2011, 2014). Ideally, for our application, we should combine an anisotropic dispersal kernel and a group dispersal model to gain in realism. However, parameter estimation may become cumbersome if the model becomes too flexible with respect to the amount of information brought by data, as discussed by Allard and Soubeyrand (2012).

This discussion about more realistic dispersal kernels has to be connected with the models of the observation processes. We chose a Poisson distribution with mean Λ_S for observations in source fields and a negative binomial distribution with mean Λ_T for observations in target fields to counterbalance the higher smoothness level of Λ_T compared with the smoothness level of Λ_S (see Material and Methods section). If a more realistic dispersal kernel is used, in particular a stochastic dispersal kernel, it may be possible to use the same distribution (e.g. Poisson) for observations in source and target fields. Incorporating a stochastic dispersal kernel into our model would be a great achievement from an epidemiological viewpoint but would lead to estimation difficulties due to the incorporation of supplementary latent variables [e.g. see the stochastic and anisotropic dispersal kernel of Soubeyrand *et al.* (2007a) and the stochastic and grouped dispersal kernel

of Soubeyrand *et al.* (2011)]. These supplementary latent variables have been handled in an estimation procedure for a situation with a single point source of inoculum (Soubeyrand *et al.*, 2007a). However, in our case where there are multiple sources whose infection strengths are estimated, we believe that the existing estimation methods, the limited amount of information in data and the absence of accurate prior knowledge do not allow us, today, to cope with the supplementary latent variables accompanying the use of a stochastic dispersal kernel.

Regarding the estimation of model parameters, the use of vague prior distributions can lead to instability in MCMC-based computations of posterior distributions. We have not encountered such instability in the analysis presented in this article. However, when we fitted to data more flexible models than the model presented in this article, the MCMC algorithm was unstable (e.g. when σ_3 and β_2 were not fixed). Using informative prior distributions could be a way to solve convergence issues. Such informative prior distributions could be built by exploiting results presented in this article and used for fitting flexible models to other data sets dealing with the dispersal of *L. maculans* ascospores.

In the Results section, we evoked meteorological variables to describe the study sites. Correlating meteorology and dispersal pattern is difficult when one only has at disposal a few observed dispersal patterns (two patterns in this article). However, in further studies, meteorological data could be incorporated as explanatory variables in our model, like in Soubeyrand *et al.* (2009a) where infection strength and survival probability are nonlinear functions of covariates and the effect of these covariates is estimated. In our case, parameter μ that partially determines the strength of sources could be written as a function integrating temperature and humidity across the time period separating the two samples (in source and target fields). Moreover, if an anisotropic version of our model is developed, dispersal parameters could be written as functions integrating wind data, like in Klein *et al.* (2003).

Given the dispersal kernel obtained from our dataset, the major recommendation for disease management is to avoid cropping oilseed rape in fields adjacent to fields with previous year's stubble, which has been left unincorporated. Based on an Australian study, previous recommendations were to sow oilseed rape at distances greater than 100 m, preferably 500 m (Marcroft *et al.*, 2004). Our results support these recommendations. Further, the combination of the dispersal kernel with integration of particle flow over polygons (e.g. with the Califlopp program; Bouvier *et al.*, 2009) opens the way to producing risk maps over landscapes. Further, the availability of this empirical dispersal kernel opens the way to find a scale at which the spatial heterogeneity of the landscape is unfavourable to disease dispersal, or maximising the likelihood of success for management interventions, according to the disease scaling hypothesis (Skelsey *et al.*, 2013).

Acknowledgements

We thank Farmers near Le Rheu who allowed us to assess disease in their fields. We thank Claude Domin, Arnaud Ribulé and Hervé Douchy for technical assistance. This work benefited from the financial support of INRA – the French National Institute for Agronomical Research –, from ANR – the French National Research Agency – programs Agriculture et Développement Durable grant ANR-05-PADD-05, CEDRE, AGROBIOSPHERE grant ANR-11-AGRO-003-01, GESTER and from the European Union Seventh Framework Programme (PLANTFOODSEC, 261752). The authors declare the absence of conflict of interest.

Supplementary Materials

aab12205-sup-0001-FigureS1.pdfPS document, 368.5 KB	**Fig. S1.** Mean and cumulative temperature, rainfall and wind distance per month in cropping seasons from 2009–2010 to 2012–2013. Wind distance is calculated as the product of duration by intensity. Data were obtained from the INRA CLIMATIK database, for Le Rheu weather station, on an hourly basis.
aab12205-sup-0002-FigureS2.pdfPS document, 208 KB	**Fig. S2.** Mean hourly wind distance (km) per autumn (from 1 September to November 30) for autumns 2009–2012. Wind distance is calculated as the product of duration by intensity. Data were obtained from the INRA CLIMATIK database, for Le Rheu weather station, on an hourly basis.

aab12205-sup-0003-FigureS3.pdfPS document, 318.5 KB

Fig. S3. Cumulative potential distance travelled by spores (km) per month in September, October and November for autumns 2009–2012 in the landscape represented in Figs 2 and 3. Potential travelled distance is calculated as the product of wind duration by intensity, for each of eight directions. Data were obtained from the INRA CLIMATIK database, for Le Rheu weather station, on an hourly basis. For the ease of reading, a different colour is used for each season.

aab12205-sup-0004-FigureS4.pdfPS document, 122 KB

Fig. S4. Posterior distribution of parameters of the model fitted to 2009–2010 data.

aab12205-sup-0005-FigureS5.pdfPS document, 116.5 KB

Fig. S5. Posterior distribution of parameters of the model fitted to 2011–2012 data.

aab12205-sup-0006-FigureS6.pdfPS document, 272.8 KB

Fig. S6. Observed disease measurements versus model predictions for source plots (top left panel) and target plots (bottom left panel) for the 2009–2010 data set. The model predictions correspond to the posterior medians (circles) of the disease measurements and their 95% posterior intervals (endpoints of grey vertical segments correspond to the 2.5% and 97.5% posterior quantiles). Circles drawn in blue (resp. green) correspond to observed disease measurements whose prediction is too small (resp. too large) (i.e. observed disease measurement is not in the corresponding 95% posterior intervals). The blue and green circles are represented in space in the right panels.

aab12205-sup-0007-FigureS7.pdfPS document, 272.1 KB

Fig. S7. Observed disease measurements versus model predictions for source plots (top left panel) and target plots (bottom left panel) for the 2011–2012 data set. The model predictions correspond to the posterior medians (circles) of the disease measurements and their 95% posterior intervals (endpoints of grey vertical segments correspond to the 2.5% and 97.5% posterior quantiles). Circles drawn in blue (resp. green) correspond to observed disease measurements whose prediction is too small (resp. too large) (i.e. observed disease measurement is not in the corresponding 95% posterior intervals). The blue and green circles are represented in space in the right panels.

aab12205-sup-0008-FigureS8.pdfPS document, 154.6 KB

Fig. S8. Observed disease measurements versus model predictions for target plots (left), for the 2009–2010 data set. The model predictions correspond to the posterior medians (circles) of the disease measurements and their 95% posterior intervals (endpoints of grey vertical segments correspond to the 2.5% and 97.5% posterior quantiles). Circles drawn in blue correspond to large observed disease measurements (greater than 50) whose predictions are generally smaller in expectation. The blue circles are represented in space in the right panel.

aab12205-sup-0009-TableS1.docWord document, 28.5 KB

Table S1. Prior distributions and proposal distributions of model parameters (or their logarithms).

aab12205-sup-0010-TableS2.docWord document, 81 KB

Table S2. Assessment of prediction performance in source and target plots for the 2009–2010 and 2011–2012 data sets, with sample sizes and coverage rates of disease measurements by their 95% posterior intervals. For each disease measurement, we computed a 95% posterior interval based on parameter posterior distributions and the randomness of the observation process (Poisson randomness for measurements in source plots; negative binomial randomness for measurements in target plots). The coverage of a disease measurement by its 95% posterior interval is a binary variable that is equal to 1 if the measurement is included in the interval, 0 otherwise. The coverage rate is the proportion of disease measurements for which the binary variable is equal to 1.

Please note: The publisher is not responsible for the content or functionality of any supporting information supplied by the authors. Any queries (other than missing content) should be directed to the corresponding author for the article.

References

Allard D., Soubeyrand S. (2012) Skew-normality for climatic data and dispersal models for plant epidemiology: when application fields drive spatial statistics. *Spatial Statistics*, 1, 50–64.

Aubertot J.N., Pinochet X., Doré T. (2004) Analysis of the effects of sowing date and nitrogen availability during vegetative stages on phoma stem canker (*Leptosphaeria maculans*) development on two winter oilseed rape cultivars. *Crop Protection*, 23, 635–645.

Austerlitz F., Dick C.W., Dutech C., Klein E.K., Oddou-Muratorio S., Smouse P.E., Sork V.L. (2004) Using genetic markers to estimate the pollen dispersal curve. *Molecular Ecology*, 13, 937–954.

Beckie H.J., Hall L.M. (2008) Simple to complex: modelling crop pollen-mediated gene flow. *Plant Science*, 175, 615–628.

Berliner L.M. (2003) Physical-statistical modeling in geophysics. *Journal of Geophysical Research*, 108, 8776–8785.

Bokor A., Barbetti M.J., Brown A.G.P., MacNish G.C., Wood P.M. (1975).Blackleg of rapeseed. *Journal of Agriculture, Western Australia* 16, 7–10.

Bourgeois A., Gaba S., Munier-Jolain N., Borgy B., Monestiez P., Soubeyrand S. (2012) Inferring weed spatial distribution from multi-type data. *Ecological Modelling*, 226, 92–98.

Bousset L., Chèvre A.M. (2012) Controlling cyclic epidemics on the crops of the agro-ecosystems: articulate all the dimensions in the formalisation, but look for a local solution. *Journal of Botany*, 2012, 9.

Bousset L., Chèvre A.M. (2013) Stable epidemic control in crops based on evolutionary principles: adjusting the metapopulation concept to agro-ecosystems. *Agriculture, Ecosystems and Environment*, 165, 118–129.

Bouvier A., Kiêu K., Adamczyk K., Monod H. (2009) Computation of the integrated flow of particles between polygons. *Environmental Modelling and Software*, 24, 843–849.

Broquet T., Petit E.J. (2009) Molecular estimation of dispersal for ecology and population genetics. *Annual Review of Ecology, Evolution, and Systematics*, 40, 193–216.

Brun H., Chèvre A.M., Fitt B.D.L., Powers S., Besnard A.L., Ermel M., Huteau V., Marquer B., Eber F., Renard M., Andrivon D. (2010) Quantitative resistance increases the durability of qualitative resistance to *Leptosphaeria maculans* in *Brassica napus*. *New Phytologist*, 185, 285–299.

Damgaard C., Kjellsson G. (2005) Gene flow in oilseed rape (*Brassica napus*) according to isolation distance and buffer zone. *Agriculture, Ecosystems and Environnement*, 108, 291–301.

Delourme R., Chèvre A.M., Brun H., Rouxel T., Balesdent M.H., Dias J.S., Salisbury P., Renard M., Rimmer S.R. (2006) Major gene and polygenic resistance to *Leptosphaeria maculans* in oilseed rape (*Brassica napus*). *European Journal of Plant Pathology*, 114, 41–52.

Diggle P.J., Moyeed R.A., Tawn J.A. (1998) Model-based geostatistics. *Journal of the Royal Statistical Society – Series C: Applied Statistics*, 47, 299–350.

Diggle A.J., Salam M.U., Thomas G.J., Yang H.A., O'Connell M., Sweetingham M.W. (2002) AnthracnoseTracer: a spatiotemporal model for simulating the spread of anthracnose in a lupin field. *Phytopathology*, 92, 1110–1121.

Dilmaghani A., Balesdent M.H., Didier J.P., Wu C., Davey J., Barbetti M.J., Li H., Moreno-Rico O., Phillips D., Despeghel J.P., Vincenot L., Gout L., Rouxel T. (2009) The *Leptosphaeria maculans–Leptosphaeria biglobosa* species complex in the American continent. *Plant Pathology*, 58, 1044–1058.

Ghanbarnia K., Fernando W.G.D., Crow G. (2009) Developing rainfall- and temperature-based models to describe infection of canola under field conditions caused by pycnidiospores of *Leptosphaeria maculans*. *Phytopathology*, 99, 879–886.

Ghanbarnia K., Fernando D.W.G., Crow G. (2011) Comparison of disease severity and incidence at different growth stages of naturally infected canola plants under field conditions by pycnidiospores of *Phoma lingam* as a main source of inoculum. *Canadian Journal of Plant Pathology*, 33, 355–363.

Gregory P. (1968) Interpreting plant disease dispersal gradients. *Annual Review of Phytopathology*, 6, 189–212.

Hammond K.E., Lewis B.G. (1986) The timing and sequence of events leading to stem canker disease in populations of Brassica napus var. *oleifera* in the field. *Plant Pathology*, 35, 551–564.

Holmes N.S., Morawska L. (2006) A review of dispersion modelling and its application to the dispersion of particles: an overview of different dispersion models available. *Atmospheric Environment*, 40, 5902–5928.

Hossard L., Jeuffroy M.H., Pelzer E., Pinochet X., Souchère V. (2013) A participatory approach to design spatial scenarios of cropping systems and assess their effects on phoma stem canker management at a regional scale. *Environmental Modelling and Software*, 48, 17–26.

Kass R.E., Raftery A.E. (1995) Bayes factors. *Journal of the American Statistical Association*, 90, 773–795.

Klein E.K., Lavigne C., Foueillassar X., Gouyon P.H., Larédo C. (2003) The corn pollen dispersal: mechanistic models and field experiments. *Ecological Monographs*, 73, 131–150.

Leflon M. (2013) Phoma du colza : la résistance spécifique Rlm7 perd de son efficacité. *Perspectives Agricoles*, 399, 58–61.

Lô-Pelzer E., Aubertot J.N., David O., Jeuffroy M.H., Bousset L. (2009) Relationship between the severity of blackleg (*Leptosphaeria maculans/L. biglobosa* complex) and subsequent primary inoculum production on oilseed rape stubble. *Plant Pathology*, 58, 61–70.

Lô-Pelzer E., Bousset L., Jeuffroy M.H., Salam M.U., Pinochet X., Boillot M., Aubertot J.N. (2010) SIPPOM-WOSR: a simulator for integrated pathogen population management of phoma stem canker on winter oilseed rape. I. Description of the model. *Field Crops Research*, 118, 73–81.

Marcroft S.J., Sprague S.J., Pymer S.J., Salisbury P.A., Howlett B.J. (2004) Crop isolation, not extended rotation length, reduces blackleg (*Leptosphaeria maculans*) severity of canola (*Brassica napus*) in south-eastern Australia. *Australian Journal of Experimental Agriculture*, 44, 601–606.

Marin J.M., Robert C.P. (2007) Bayesian Core: A Practical Approach to Computational Bayesian Statistics, Springer Texts in Statistics. New York, NY, USA: Springer.

McHardy W.E. (1997) Ascospore dispersal and deposition. In Apple Scab Biology, Epidemiology and Management, pp. 293–306. Ed W.E. McHardy. St Paul, MN, USA: APS Press.

Mendes-Pereira E., Balesdent M.H., Brun H., Rouxel T. (2003) Molecular phylogeny of the *Leptosphaeria maculans–L. biglobosa* species complex. *Mycological Research*, 107, 1287–1304.

Mundt C.C., Sackett K.E., Wallace L.D., Cowger C., Dudley J.P. (2009) Long distance dispersal and accelerating waves of disease: empirical relationships. *American Naturalist*, 173, 456–466.

Mundt C.C., Sackett K.E., Wallace L.D. (2010) Landscape heterogeneity and disease spread: experimental approaches with a plant pathogen. *Ecological Applications*, 21, 321–328.

Pinochet X. (2009) Colza : gérer les variétés dans la lutte contre le phoma. *Perspectives Agricoles*, 357, 90–92.

Rieux A. (2011) Etude des processus de dispersion et des flux géniques chez un champignon phytopathogène : le cas de Mycosphaerella fijiensis à l'échelle d'un bassin de production camerounais. PhD Thesis, SupAgro, Montpellier, France.

Rieux A., Lenormand T., Carlier J., de Lapeyre de Bellaire L., Ravigné V. (2013) Using neutral cline decay to estimate contemporary dispersal: a generic tool and its application to a major crop pathogen. *Ecology Letters*, 16, 721–730.

Rieux A., Soubeyrand S., Bonnot F., Klein E.K., Ngando J.E., Mehl A., Ravigne V., Carlier J., de Lapeyre de Bellaire L. (2014) Long-distance wind-dispersal of spores in a fungal plant pathogen: estimation of anisotropic dispersal kernels from an extensive field experiment. *PLoS One*, 9, e103225.

Rousset F. (1997) Genetic differentiation and estimation of gene flow from F-statistics under isolation by distance. *Genetics*, 145, 1219–1228.

Sackett K.E., Mundt C.C. (2005) Primary disease gradients of wheat stripe rust in large field plots. *Phytopathology*, 95, 983–991.

Sackett K.E., Mundt C.C. (2009) Effect of plot geometry on epidemic velocity of wheat yellow rust. *Plant Pathology*, 58, 370–377.

Savage D., Barbetti M.J., MacLeod W.J., Salam M.U., Renton M. (2011) Can mechanistically parameterised, anisotropic dispersal kernels provide a reliable estimate of wind-assisted dispersal? *Ecological Modelling*, 222, 1673–1982.

Savage D., Barbetti M.J., MacLeod W.J., Salam M.U., Renton M. (2012) Seasonal and diurnal patterns of spore release can significantly affect the proportion of spores expected to undergo long-distance dispersal. *Microbial Ecology*, 63, 578–585.

Savage D., Barbetti M.J., MacLeod W.J., Salam M.U., Renton M. (2013) Temporal patterns of ascospore release in *Leptosphaeria maculans* vary depending on geographic region and time of observation. *Microbial Ecology*, 65, 584–592.

Skelsey P., Holtslag A.A.M., van der Werf W. (2008) Development and validation of a quasi-Gaussian plume model for the transport of botanical spores. *Agricultural and Forest Meteorology*, 148, 1383–1394.

Skelsey P., Kessel G.J.T., Holtslag A.A.M., Moene A.F., van der Werf W. (2009) Regional spore dispersal as a factor in disease risk warnings for potato late blight: a proof of concept. *Agricultural and Forest Meteorology*, 149, 419–430.

Skelsey P., With K.A., Garrett K.A. (2013) Pest and Disease management: why we shouldn't go against the grain. *PLoS One*, 8, e75892.

Soubeyrand S., Enjalbert J., Sanchez A., Sache I. (2007a) Anisotropy, in density and in distance, of the dispersal of yellow rust of wheat: experiments in large field plots and estimation. *Phytopathology*, 97, 1315–1324.

Soubeyrand S., Thébaud G., Chadœuf J. (2007b) Accounting for biological variability and sampling scale: a multi-scale approach to building epidemic models. *Journal of the Royal Society Interface*, 4, 985–997.

Soubeyrand S., Laine A.-L., Hanski I., Penttinen A. (2009a) Spatio-temporal structure of host-pathogen interactions in a metapopulation. *The American Naturalist*, 174, 308–320.

Soubeyrand S., Neuvonen S., Penttinen A. (2009b) Mechanical-statistical modeling in ecology: from outbreak detections to pest dynamics. *Bulletin of Mathematical Biology*, 71, 318–338.

Soubeyrand S., Enjalbert J., Kretzschmar A., Sache I. (2009c) Building anisotropic sampling schemes for the estimation of anisotropic dispersal. *Annals of Applied Biology*, 154, 399–411.

Soubeyrand S., Roques L., Coville J., Fayard J. (2011) Patchy patterns due to group dispersal. *Journal of Theoretical Biology*, 271, 87–99.

Soubeyrand S., Mrkvicka T., Penttinen T. (2014) A nonstationary cylinder-based model describing group dispersal in a fragmented habitat. *Stochastic Models*, 30, 48–67.

Travadon R., Bousset L., Saint-Jean S., Brun H., Sache I. (2007) Splash dispersal of *Leptosphaeria maculans* pycnidiospores and the spread of blackleg on oilseed rape. *Plant Pathology*, 56, 595–603.

Travadon R., Sache I., Dutech C., Stachowiak A., Marquer B., Bousset L. (2011) Absence of isolation by distance patterns at the regional scale in the fungal plant pathogen *Leptosphaeria maculans*. *Fungal Biology*, 115, 649–659.

Turkington T.K., Clayton G.W., Klein-Gebbinck H., Woods D.L. (2000) Residue decomposition and blackleg of canola: influence of tillage practices. *Canadian Journal of Plant Pathology*, 22, 150–154.

Viljanen-Rollinson S.L.H., Parr E.L., Marroni M.V. (2007) Monitoring long-distance spore dispersal by wind – a review. *New Zealand Plant Protection*, 60, 291–296.

West J.S., Kharbanda P.D., Barbetti M.J., Fitt B.D.L. (2001) Epidemiology and management of *Leptosphaeria maculans* (phoma stem canker) on oilseed rape in Australia, Canada and Europe. *Plant Pathology*, 50, 10–27.

Wikle C.K. (2003) Hierarchical Bayesian models for predicting the spread of ecological processes. *Ecology*, 84, 1382–1394.

Wingen L.U., Shaw M.W., Brown J.K.M. (2013) Long-distance dispersal and its influence on adaptation to host resistance in a heterogeneous landscape. *Plant Pathology*, 62, 9–20.

Xhaard C., Barrès B., Andrieux A., Bousset L., Halkett F., Frey P. (2012) Disentangling the genetic origins of a plant pathogen during disease spread using an original molecular epidemiology approach. *Molecular Ecology*, 21, 2383–2398.

Yaglom A.M. (1987) Correlation Theory of Stationary and Related Random Functions I Basic Results, pp. 526. New York, NY, USA: Springer-Verlag.

Zadoks J.C., Schein R.D. (1979) Epidemiology and Plant Disease Management, pp. 427. New York, NY, USA: Oxford University Press.

Zhang X., White R.P., Demir E., Jedryczka M., Lange R.M., Islam M., Li Z.Q., Huang Y.J., Hall A.M., Zhou G., Wang Z., Cai X., Skesley P., Fitt B.D.L. (2014) *Leptosphaeria* spp., phoma stem canker and potential spread of *L. maculans* on oilseed rape crops in China. *Plant Pathology*, 63, 598–612.